*Journal of GeoEngineering, Vol. 11, No. 2, pp. 75-83, August 2016*
*http://dx.doi.org/10.6310/jog.2016.11(2).3*


# UNDRAINED CAPACITY OF LATERALLY LOADED UNDERGROUND WALLS SUBJECTED TO HORIZONTAL LOAD AND MOMENT

Suraparb Keawsawasvong [1] and Boonchai Ukritchon [2*]

## ABSTRACT

In engineering practice, underground walls, such as concrete diaphragm walls, are conventionally employed for constructions of deep excavations, basements, underpasses, cut-and-cover tunnels, *etc*. These walls may be subjected to combined horizontal load ($H$) and moment ($M$) that arise from external forces to support a permanent superstructure or a temporary platform of deep excavations. A new numerical solution of undrained capacity of laterally loaded walls under static conditions of combined horizontal load and moment is presented, which can be applied for predicting laterally loaded capacity of an underground wall with a sufficient horizontal length. The 2D plane strain finite element analysis is employed to determine the limit load of this problem. Dimensional parameters of the problem include undrained shear strength ($s_u$) of clay layer, unit weight of soil ($\gamma$), and embedded length of wall ($L$). The embedded wall is modeled as an elastic material without failure consideration, while the clay is modeled as the Tresca material in an undrained condition. Results are summarized in the form of failure envelope of dimensionless variables as horizontal load factor and moment factor as a function of overburden factor. Associated failure mechanisms corresponding to dimensionless variables are also presented in the paper. It was found that for the case of no tension, the undrained lateral capacity of purely horizontal load ranges from $H/s_uL$ = 1.1 to 2.0 while that of pure moment ranges from $M/s_uL^2$ = 0.7 to 1.3. In addition, the failure envelope of walls subjected to combined horizontal load and moment has the form of rotated ellipse with distortion at both ends. The size of failure envelope is controlled by the overburden pressure factor, $\gamma_sL/s_u$. The increase of $\gamma_sL/s_u$ results in the increase of size of failure envelope until it converges to that of the full tension case, whose the failure envelope is unaffected by $\gamma_sL/s_u$.

*Key words:* Finite element, embedded walls, combined loading, plane strain.

## 1. INTRODUCTION

Pile foundations of complex structures such as offshore structures, bridges, or high-rise buildings generate a more complex loading in addition to a vertical load case. Loading considerations should include horizontal load direction as well as overturning moment in order to model the most realistic and critical case. In a real situation, forces acting on those structures arise from wave forces, wind loadings, or dynamics forces from earthquake actions. Such actions can generate combined horizontal load and moment acting on the top of piles.

A large number of studies on laterally loaded piles have been carried out in the past to understand and determine lateral capacity of piles. The methods of analysis of lateral piles include: (1) limit equilibrium method (*e.g.* Blum 1932; Broms 1964; Broms 1965); (2) subgrade reaction method or Winkler spring method (*e.g.* Matlock and Reese 1960, Davisson and Gill 1963); (3) the *p-y* curve (*e.g.* Reese *et al*. 1974; Reese 1977; Wang and Reese 1993; Ismael 1990; Reese *et al*. 2000); (4) the elastic continuum approach using boundary element method (*e.g.* Poulos and Davis 1980; Zhang and Small 2000; Shen and Teh 2002); and (5) finite element method (*e.g.* Muqtadir and Desai 1986; Brown and Shie 1991; Trochanis *et al*. 1991; Kimura *et al*. 1995; Yang and Jeremic 2002; Yang and Jeremic 2005). Ruigrok (2010) and Reese *et al*. (2007) reviewed advantages and disadvantages of available methods of calculation for a lateral resistance of piles.

One of the oldest and classical methods for analyzing an ultimate lateral resistance of piles was proposed by Blum (1932) and Broms (1964, 1965). Even though those two methods can be used to determine an ultimate lateral resistance of piles, they are different in theoretical background in modeling lateral soil resistance using simple geometrical earth pressure distribution. As a result, calculations of both Blum's and Broms's methods may be incorrect and not accurate. In addition, Blum's method does not take into account of undrained shear strength in the calculation, thus it may be difficult to apply his method when dealing with an analysis of lateral capacity of piles in cohesive soils.

At present, numerical methods are more advanced than those in the past. The finite element method has become popular in analyzing an ultimate resistance of a pile. Chaudhry (1994), Klar (2008), and Zhang (2011) employed a finite element analysis for piles under a lateral load. However, their results are not summarized in the form of dimensionless variables or the design chart of failure envelope. An example of previous studies of failure envelope include Ukritchon *et al*. (1998) who considered the limit state solution of a strip footing subjected to vertical and horizontal loads and moment.

Manuscript received February 15, 2016; revised April 11, 2016; accepted June 8, 2016.
[1] Research Assistant, Geotechnical Research Unit, Department of Civil Engineering, Faculty of Engineering, Chulalongkorn University, Bangkok 10330, Thailand.
[2] Associate Professor (corresponding author), Geotechnical Research Unit, Department of Civil Engineering, Faculty of Engineering, Chulalongkorn University, Bangkok 10330, Thailand (e-mail: boonchai.uk@gmail.com).

Underground walls are conventionally found in engineering practice, such as concrete diaphragm walls that are used for constructions of deep excavations, basements, underpasses, cut-and-cover tunnels, *etc*. These walls may be subjected to combined horizontal load and moment that arise from external forces to support a permanent superstructure or a temporary platform of deep excavations. Thus, this paper aims to study a prediction of undrained lateral capacity of a wall subjected horizontal load and moment under static conditions since its stability assessment are essential to ensure an adequate safety factor of a wall against such loadings. The results in this study can be applied to predict the lateral capacity of underground walls having a sufficient horizontal length in practice.

As described earlier, various previous works have been performed to study lateral capacity of piles. However, there are very few studies on laterally loaded walls in the literature. Ukritchon (1998) and Huang *et al*. (2007) applied finite element limit analysis to determine the failure envelope for embedded walls under horizontal load and moment by assuming the plane strain condition. However, their results were based on the modeling of soil as a weightless material ($\gamma_s = 0$). Thus, their solutions have a very limited application in practice since it cannot be used for problems with the presence of soil unit weight ($\gamma_s \neq 0$). In this study, the continuum approach, finite element method, is adopted to model a laterally loaded wall since a realistic prediction of undrained lateral capacity of a wall can be achieved by this simulation, particularly for considering an influence of soil unit weight and the soil-pile interactions as full tension and/or no tension cases on the limit load.

This paper presents new finite element solutions of undrained lateral capacity of underground walls under a horizontal load and moment. It is assumed that the wall has a sufficient horizontal length such that the two dimensional plane strain finite element analysis can be employed to determine the limit load of this problem. Parametric studies of finite element analyses are performed to generate dimensionless variables of failure envelopes for walls under a horizontal load and moment. Unlike other previous studies in the past, the influence of soil unit weight and soil-pile interfaces as full tension and no tension will be studied extensively in this paper. Results of finite element solutions can be applied to estimate an undrained lateral capacity of underground walls with a sufficient horizontal length under a horizontal load and moment in practice. The next section explains important modelling issues and details of this study.

## 2. METHOD OF ANALYSIS

This paper employs the commercial finite element software, Plaxis 2D (Brinkgreve 2002) to simulate a numerical model and analyze an undrained lateral capacity of a wall embedded in a homogeneous clay layer. Because of the assumption of a wall with a sufficient horizontal length, the plane strain model is employed in the finite element analysis. Figure 1 shows the problem definition of this study while a corresponding numerical model is shown Fig. 2.

A homogeneous clay layer is modeled as the volume element with the Tresca material in an undrained condition and the associated flow rule. Its parameters include undrained shear strength ($s_u$), undrained Young's modulus, $E_u = 500s_u$, Poisson's ratio ($\nu$) = 0.495, total friction angle ($\phi$) = 0, total dilation angle ($\psi$) = 0. In the study, there is no consideration of the ground water level since the undrained condition with the total stress analysis is employed in the finite element calculations.

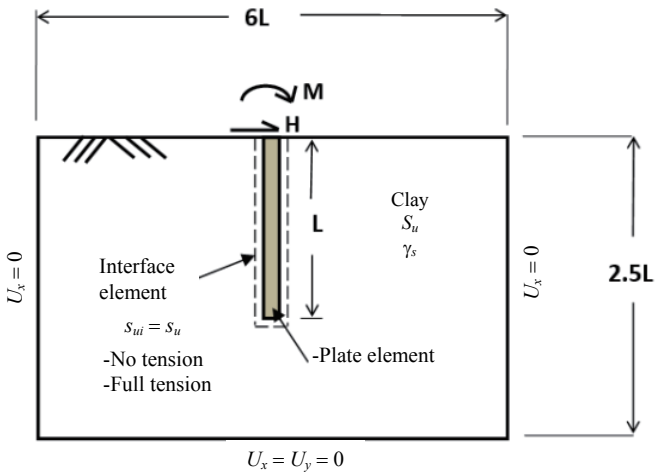


**Fig. 1 Problem geometry for combined horizontal load and moment acting on an embedded wall in clay**

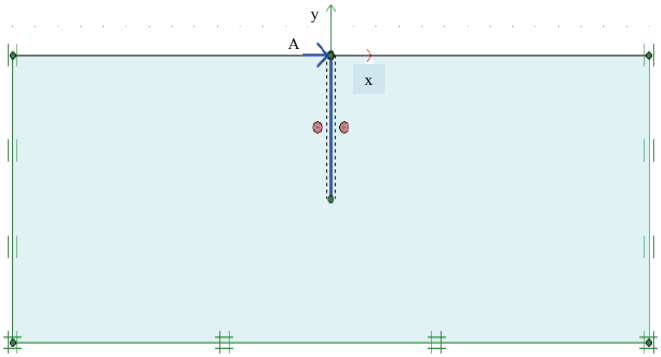


**Fig. 2 Model geometry of laterally loaded wall by Plaxis2D**

In contrast to previous works by Ukritchon (1998) and Huang *et al*. (2007) who assumed a weightless soil ($\gamma_s = 0$) for laterally loaded walls, this study considers constant soil properties with a non-zero total unit weight ($\gamma_s \neq 0$), which is generally found practice. Note that for a general soil profile, its undrained shear strength and undrained Young's modulus increase with the depth from the ground surface. This aspect of soil non-homogeneity is not taken into a consideration in the study. The assumption of constant soil properties is made in the analysis.

It is assumed that the thickness of a wall ($T$) is relatively small as compared to its vertical length ($L$) or the long wall assumption is considered in the study. Because of the long wall assumption, the wall embedded in a deep clay layer is modeled as a plate element that corresponds to a reinforced concrete with 1 m of assumed thickness with an elastic material, where Poisson's ratio = 0.21 and Young's modulus = $2.545 \times 10^7$ kPa. The assumed thickness of the wall and that Young's modulus gives rise to its bending stiffness of $2.121 \times 10^6$ kNm$^2$ per unit width of wall (in the plane strain condition) that can be considered to be relatively large to ensure its rigid behaviour. Because of a modelling of the elastic material for the embedded wall, it implies that there is no failure of the wall in the analysis. This assumption is realistic in actual design practice. The wall must be designed to have adequate dimension and reinforcement in resisting shear and bending modes such that the failure of this problem is governed by the shear strength of clay before the failure of a wall will happen.

The interaction between the clay and the wall is modeled using the soil-structure interface. These interface elements are added around both sides of the embedded wall, as shown in Figs. 1 and 2. The interface roughness between the clay and the wall is controlled by the soil-wall adhesion factor, $R_{inter}$. In this analysis, $R_{inter}$ is set as the value of 1, which corresponds to a fully rough surface of walls. According to the Tresca material, the undrained shear strength of the interface element is equal to that of the adjacent soil, *i.e.* $s_{ui} = s_u$. For embedded walls subjected to a horizontal load and moment, a separation may happen on the back side of wall. Thus, both conditions of no tension (separation case) or full tension (no separation case) are also studied. Modeling of separation case is achieved by enabling the tension cut-off for the failure criterion. On the other hand, the tension cut-off function is disabled in order to model the full tension case.

Figure 2 also shows boundary conditions of this problem that corresponds to a typical pattern used in finite element analysis in geotechnical engineering. The bottom boundary plane is defined as zero movements for both horizontal and vertical directions. The left and right boundary planes are defined as zero horizontal movement, while only its vertical movement is allowed. Several trials and errors were performed in finite element analyses to come up with an optimal size of the horizontal and vertical sizes of domain as 6$L$ and 2.5$L$, respectively. In particular, the incremental shear strain contours obtained from analyses must be checked such that they do not intersect the boundary domain. The selected domain size must be large enough to capture plastic shearing in the soil and thus the limit load of the problem is not influenced by boundary conditions.

The failure envelope of an embedded wall subjected to combined horizontal load and moment is obtained by analyzing two different cases, as shown in Fig. 3. The first case corresponds to the case where horizontal load and moment produce overturning to the same direction, labeled as I in the first quadrant. The second case corresponds to the case where horizontal load and moment produce overturning to the opposite direction, labeled as II in the second quadrant. The remaining of the graphs in the third and fourth quadrants are obtained from the symmetry of the problem. In particular, the result of the first quadrant is equal to that of the third quadrant, while that of the fourth quadrant is equal to that of the second quadrant. The failure envelope is plotted as a function of dimensionless horizontal load factor, $H/s_uL$ and dimensionless moment factor, $M/s_uL^2$. The ratio of moment to horizontal load is defined as $M/HL = \tan(\beta)$ or $M = \tan(\beta)HL$, where β is the angle which is measured from the +$x$-axis as shown in Fig. 4. To develop the failure envelope for a given value of $\gamma_sL/s_u$, the value of β is chosen from the range of 0° ~ 180° with an interval of 5° and used to define a constraint of loading in the finite element analysis. For example, let β = 30°, $L$ = 5 m., the constraint of the loading is: $M = \tan(30)(5)H = 2.887H$. This constraint is enforced in the elasto-plastic finite element calculations such that the horizontal load and moment are increased proportionally (*i.e.* $M = 2.887H$) until the limit state is reached in the simulation.

An embedded wall is loaded at the top with the horizontal load, $H$ and the moment, $M$. There are five dimensional parameters of the laterally loaded wall, namely $H$, $M$, $L$, $s_u$, and $\gamma_s$. However, the dimensionless technique (Butterfield 1999) can decrease the number of parameters from five dimensional parameters to three dimensionless parameters, namely (1) the horizontal load factor, $H/s_uL$; (2) moment factor, $M/s_uL^2$; and (3) the overburden factor, $\gamma_sL/s_u$. Note that the horizontal load and moment represent the failure values at the limit state, where they are obtained from the finite element analysis using the following input variables, $L$ = 5 m, $\gamma_s$ = 20 kPa. To perform a parametric study of $\gamma_sL/s_u = a$, an undrained shear strength is inputted as: $s_u = \gamma_sL/a$. Even though the computed horizontal failure load and/or failure moment depend on $L$, $\gamma_s$, $s_u$, the dimensionless parameters, $H/s_uL$, $M/s_uL^2$ and $\gamma_sL/s_u$ have their own unique interrelationship following the dimensionless concept proposed by Butterfield (1999). Therefore, the computed scaling laws, $H/s_uL$, $M/s_uL^2$, $\gamma_sL/s_u$ can be applied to a general condition of laterally loaded walls under a horizontal load and moment in practice.

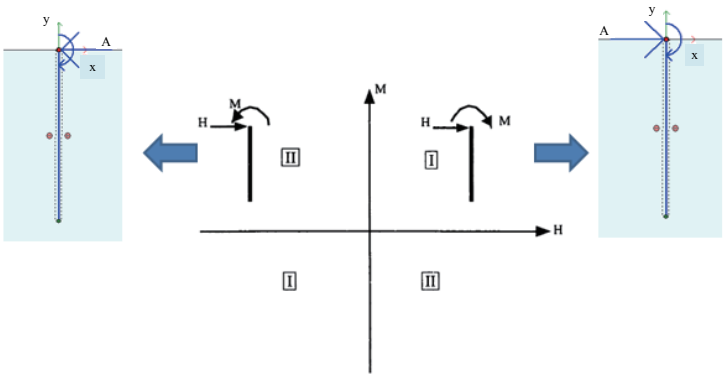


**Fig. 3 Development of failure envelope of an embedded wall subjected to combined horizontal load and moment**

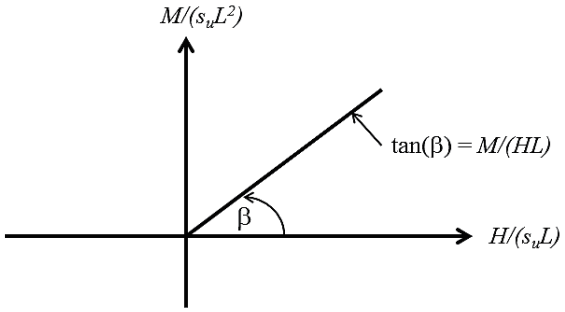


**Fig. 4 Definition of the term, β**

The results of analyses are summarized in form of dimensionless parameters of the horizontal load factor, $H/s_uL$, and moment factor, $M/s_uL^2$, as a function of overburden factor, $\gamma_sL/s_u$. Parametric studies are performed for $\gamma_sL/s_u$ = 0.5 ~ 50. For each case of the parametric study, the undrained shear strength, $s_u$, is changed while the length of wall and the unit weight of clay remain constant, giving rise to different values of $\gamma_sL/s_u$, as described earlier. It should be noted that this study presents new solutions of an embedded wall under combined horizontal load and moment with a consideration of the effect of overburden factor, $\gamma_sL/s_u$, which has not been considered in previous studies (Ukritchon 1998; and Huang *et al*. 2007).

Figure 5 shows a typical mesh used in finite element analysis of an embedded wall subjected to horizontal load and moment at its top. Triangular elements are used for modeling the clay while plate elements are used for modeling the wall. There are 15 nodes with 12 stress points and 5 nodes with 8 stress points for each triangular element and each plate element, respectively as shown in Fig. 6. In addition, a very fine mesh distribution is used in order to obtain an accurate result at the limit state. Note that

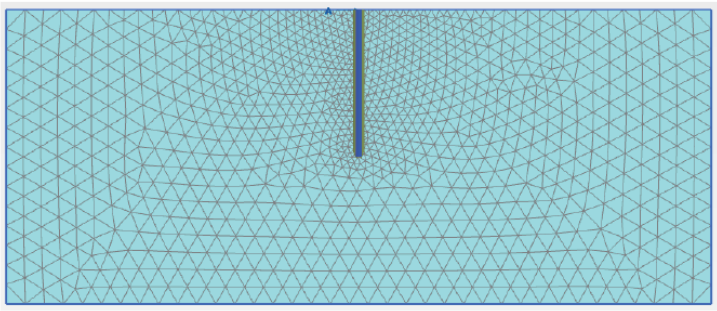

**Fig. 5 Typical mesh used in the finite element analysis**

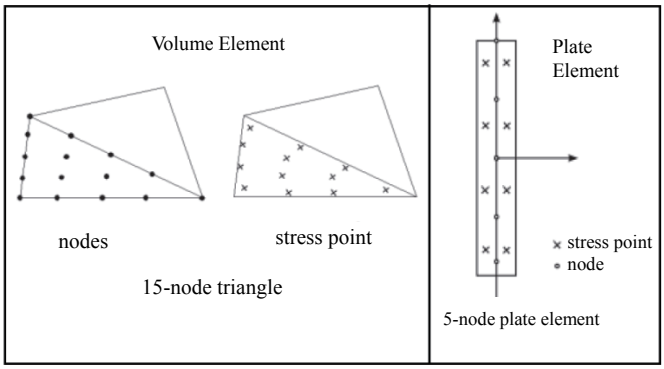


**Fig. 6 Triangular types of volume element and line types of plate element**

15-noded triangular element employs a quartic interpolation (*i.e.* 4th polynomial function) of unknown displacements, and thus is a very accurate and high performance type of element that is highly suitable for producing high quality stress field and analyzing difficult problems especially an undrained collapse problem as recommended by Sloan and Randolph (1982).

## 3. VALIDATIONS AND RESULTS

For laterally loaded walls, results of the present study are validated with existing solutions that are available only for the cases of no tension with $\gamma_s L/s_u = 0$ (*i.e.* weightless soil, $\gamma = 0$) by Ukritchon (1998) who employed the finite element upper and lower bound limit analysis. Since solutions of Huang *et al.* (2007) are identical to those of Ukritchon (1998), the former is omitted in this validation. Horizontal load, $H$ and moment, $M$ are the ultimate values obtained from finite element analyses, where they are used to compute horizontal load factor, $H/s_u L$, and moment factor, $M/s_u L^2$. Table 1 compares results of the present study with existing solutions of two cases of laterally loaded walls with no tension: (1) a purely horizontal load, and (2) a pure moment. Note that the results of present study correspond to the case of $\gamma_s L/s_u = 0.5$ since there is a numerical problem for the case of weightless material, where the solutions of the case of $\gamma = 0$ cannot be determined by finite element analysis. For the no tension case, the finite element analysis can be performed for the smallest value of $\gamma_s L/s_u = 0.5$, which is used for these validations. Even though a selected value of $\gamma_s L/s_u$ is not identical to that of Ukritchon (1998), the comparison indicates a reasonable agreement between the present study and existing solutions. Results of purely horizontal load and pure moment of the present study are slightly higher 2 ~ 3% than the upper bound solution by Ukritchon (1998).

**Table 1 Validation of the present study with existing solutions**

| Solutions | Purely horizontal load, $H/s_u L$ | Pure moment, $M/s_u L^2$ |
|---|---|---|
| Present Study | 1.210 | 0.872 |
| Ukritchon (1998), UB | 1.190 | 0.846 |
| Ukritchon (1998), LB | 1.085 | 0.764 |

Remarks: UB = upper bound, LB = lower bound

Figure 7 shows a comparison of failure envelope ($H$-$M$) for the case of combined horizontal load and moment between the present study with $\gamma_s L/s_u = 0.5$ and Ukritchon (1998) with $\gamma_s L/s_u = 0$. The shape of failure envelopes of two solutions are resemble to each other. Very clearly, existing solutions exhibit reasonable agreement with the presented study by finite element analysis, where the predicted failure envelope is slightly higher 1 ~ 10% than the upper bound solution by Ukritchon (1998).

The parametric studies of laterally loaded walls from finite element analysis show that there is the single dimensionless parameter, $\gamma_s L/s_u$, which effects on the horizontal load factor and moment factor for the no tension case. On the other hand, the term $\gamma_s L/s_u$ does not alter all output dimensionless solutions in the case of full tension.

Figure 8 shows the curves of a purely applied horizontal load ($H/s_u L$) against the normalized displacement ($y/L$), where $y$ is the displacement of the embedded wall in the same direction of the applied load. This figure shows an effect of the overburden factor on the limit load of the no tension case, where $\gamma_s L/s_u = 2$, 5, 10, 20. Note that the limit load of the full tension case is independent of $\gamma_s L/s_u$. It can be observed that the limit state of all cases is successfully simulated and solved by the finite element analysis, where all curves converge to a certain value for a very large displacement. In addition, it can be seen that an increase in the overburden factor leads to a higher capacity of purely horizontal load.

Figure 9 shows a load-displacement curve of a purely horizontal load for the no tension case, where $\gamma_s L/s_u = 10$. The vertical axis of an applied horizontal load is normalized by its computed limit load, while the horizontal axis of displacement is normalized by its corresponding movement at the failure state. Thus, this graph shows the ratio of applied load with respect to the ratio of displacement from the beginning at 0% until the failure state at 100%.

Figures 10 and 11 show incremental displacement vector and incremental shear strain, respectively, corresponding to selected applied load for the case of no tension from the beginning at 0% until the failure state at 100%, where $\gamma_s L/s_u = 10$. Note that for an analysis of the limit state condition, total displacement and total shear strain corresponding to the results of cumulative values from the initial step to the last step in the elasto-plastic calculation are meaningless since they are extremely excessive at the ultimate condition. However, incremental displacement and incremental shear strain of the last step in the elasto-plastic calculation are particularly useful to reveal failure mechanism and/or localization of deformations within the soil or shear bands when failure or limit state occurs.

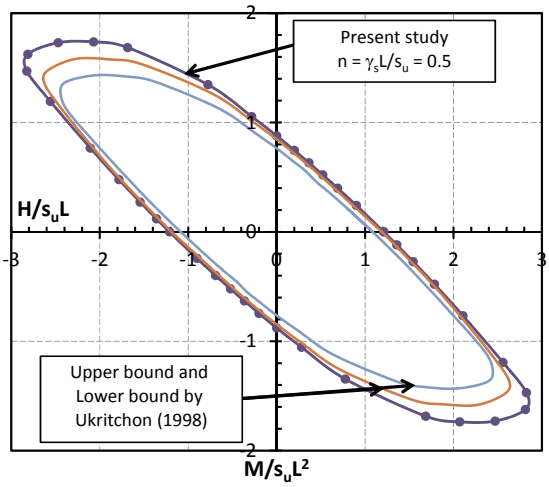


**Fig. 7 Comparison of failure envelope (*H-M*) for the case of combined horizontal load and moment between the present study with $\gamma_s L/s_u$ = 0.5 and Ukritchon (1998) with $\gamma_s L/s_u = 0$**

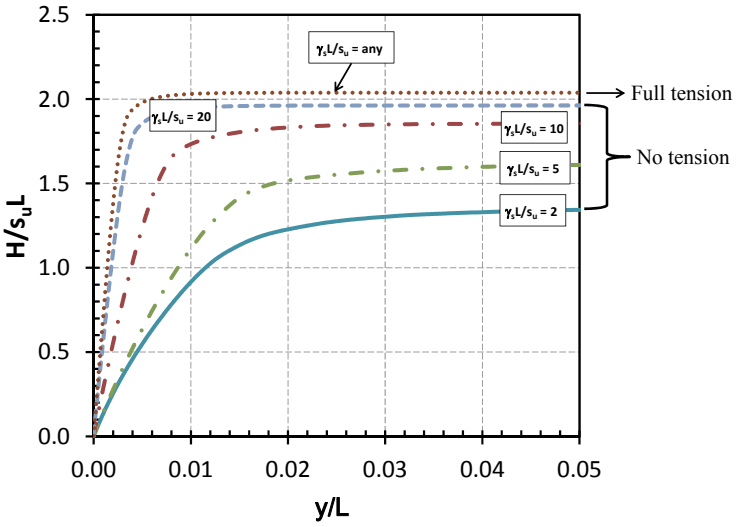


**Fig. 8 Load-displacement curves of purely horizontal load**

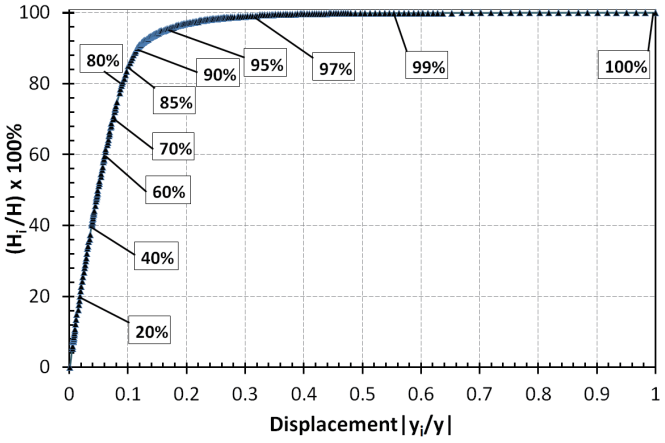


**Fig. 9 Load-displacement curve of the problem with no tension case, where $\gamma_s L/s_u = 10$**

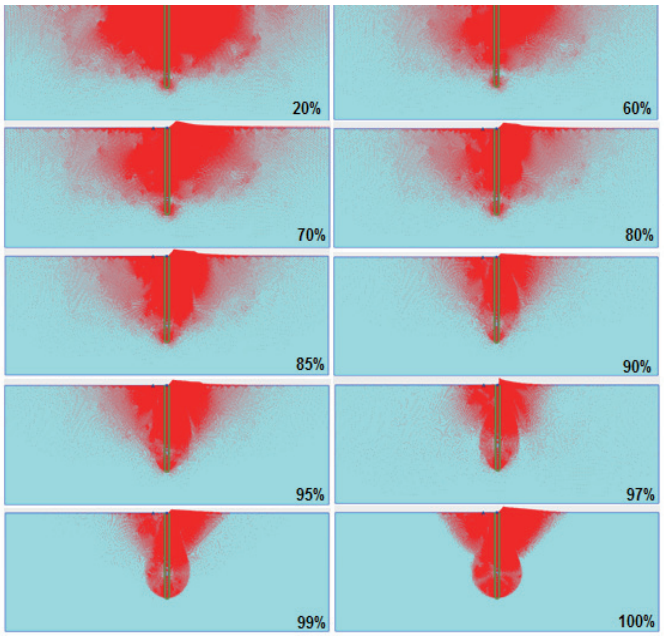


**Fig. 10 Incremental displacement of the problem with no tension case, where $\gamma_s L/s_u = 10$**

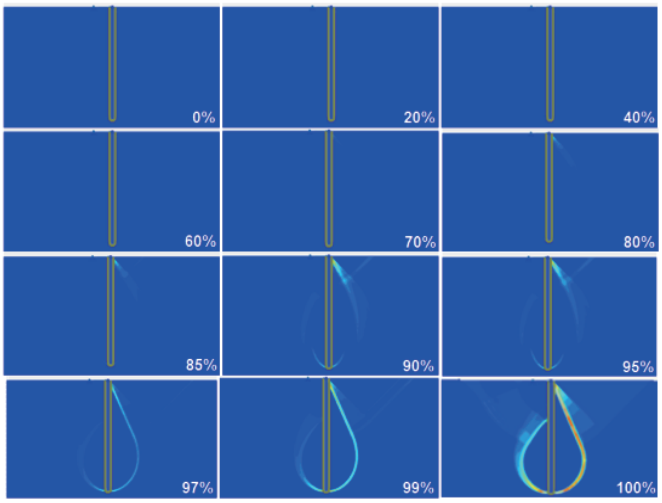


**Fig. 11 Incremental shear strain of the problem with no tension case, where $\gamma_s L/s_u = 10$**

The percentage in each subplot of Figs. 10 and 11 represents the loading ratio that is calculated from the applied horizontal load divided by the failure value. Therefore, these results show the progressive failure of a selected problem. For a loading ratio of 0 ~ 80%, there is no clear development of shear band within the soil. However, once the loading ratio reaches 90%, localized incremental displacement and shear bands start to appear in those figures. Finally, a clear failure mechanism and distinct shear bands can be seen at the limit state or the loading ratio of 100%, where "6-shaped" shear band develops from the top of wall, passes the tip of wall, and ends at the center of the back of wall.

Figures 12 and 13 show examples of predicted failure mechanisms for the case of purely horizontal load, while Figs. 14 and 15 show the results for the case of pure moment. For each case, the failure results include incremental displacement vector and incremental shear strain contour. Comparisons are made for

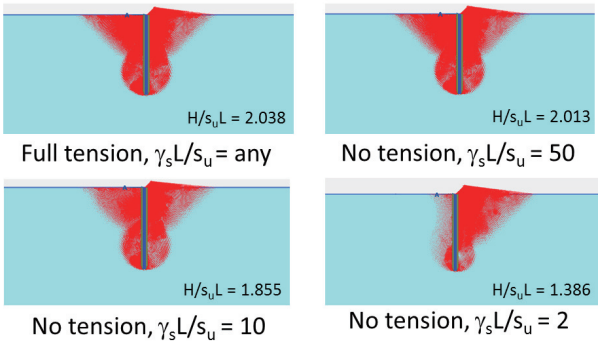


**Fig. 12 Incremental displacement for the cases of purely horizontal load**

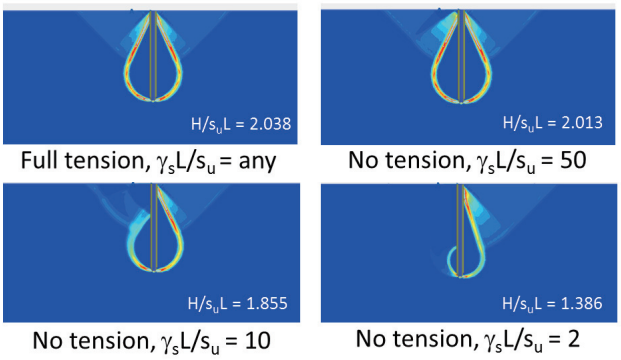


**Fig. 13 Incremental shear contours for the cases of purely horizontal load**

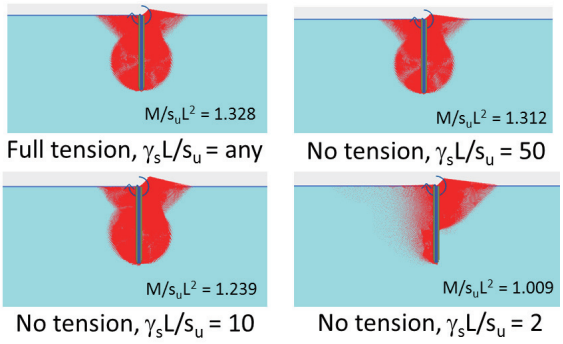


**Fig. 14 Incremental displacement for the cases of pure moment**

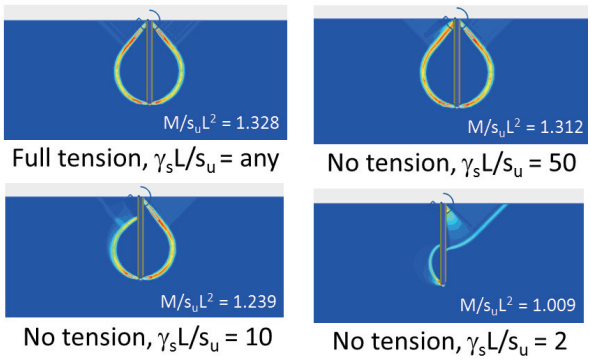


**Fig. 15 Incremental shear contours for the cases of pure moment**

three values of overburden factor of the no tension cases, where $\gamma_s L/s_u$ = 2, 10, 50, and one result of the full tension case. Note that for the full tension case, "$\gamma_s L/s_u$ = any" in Figs. 12 ~ 15 means that the solutions of this case are unaffected by the overburden factor, $\gamma_s L/s_u$, where this term can practically range from 0 ~ ∞.

It can be observed that the results of no tension case show a separation on the back side of wall. But, separation is not observed in the case of full tension. For purely horizontal load (Figs. 12 and 13), the failure mechanism of an embedded wall happens such that the wall rotates about some point near its tip without translational movement. Near the ground surface, the front side fails in the passive state condition, while the back side fails in the active mode. For the case of $\gamma_s L/s_u$ = 2 (no tension), the failure zone is concentrated on the back side near the tip of the wall. Then, an increase of $\gamma_s L/s_u$ gives rise to a more increase of failure zone on the back side of the wall. When $\gamma_s L/s_u$ reaches to ∞, the failure mechanism of no tension case becomes that of full tension, where a further increase in $\gamma_s L/s_u$ does not alter the failure mechanism. For pure moment (Figs. 14 and 15), the embedded wall fails by a rotation at about the mid-point of the wall without translational movement. The failure zones of passive and active modes of pure moment are much smaller than that of purely horizontal load.

Figures 16 and 17 show the relationships of the dimensionless parameters between horizontal load factor, $H/s_u L$, moment factor, $M/s_u L^2$, and overburden pressure factor, $\gamma_s L/s_u$. The constant line and the curvilinear line represent the full tension case and the no tension case, respectively. It can be observed that the solutions of full tension case in these figures have constant values, where $H/s_u L = 2.038$ and $M/s_u L^2 = 1.328$. For no tension case, the increase of $\gamma_s L/s_u$ gives rise to the increase of $H/s_u L$ and $M/s_u L^2$. When $\gamma_s L/s_u$ reaches to ∞, the solutions converge to those of the full tension case. It can be seen that when $\gamma_s L/s_u = 0$, the two solutions of the present study converges to those of Ukritchon (1998), where excellent agreements between all solutions can be observed. In general, the undrained lateral capacity of purely horizontal load, $H/s_u L$ increases nonlinearly from 1.1 and converges to 2.1 for a large value of overburden factor, $\gamma_s L/s_u$. Similarly, that capacity of pure moment, $M/s_u L^2$ increases nonlinearly from 0.75 and remains a constant of 1.33 for a large value of $\gamma_s L/s_u$.

Figures 18 and 19 show comparisons of failure mechanisms of the purely horizontal load case between this study and those of Ukritchon (1998). Obviously, similar characteristics of failure mechanisms between these two studies can be observed. Note that a separation can be seen on the back of wall in the two solutions.

Figure 20 shows series of failure envelopes for the cases of no tension with the overburden pressure factor, $n = \gamma_s L/s_u$ = 0.5, 2, 3, 5, 10, 50 and the case of full tension. Note that the condition of β = 0° represents a laterally loaded wall purely subjected to a horizontal load, while the condition of β = 90° represents a laterally loaded wall purely subjected to a moment. A radial distance from the origin to the point on a failure envelope denotes the total lateral capacity of a wall subjected to a horizontal load and moment. Therefore, it can be seen in the figure that the condition of β = 45°, *i.e.* $M/HL = 1$, corresponds to the smallest total lateral capacity of walls, where both a horizontal load and moment produce an overturning to the same direction. In contrast, the condition of β = 135°, *i.e.* $M/HL = -1$, corresponds to the largest total lateral capacity of walls, where both a horizontal load and moment produce an overturning to the opposite direction.

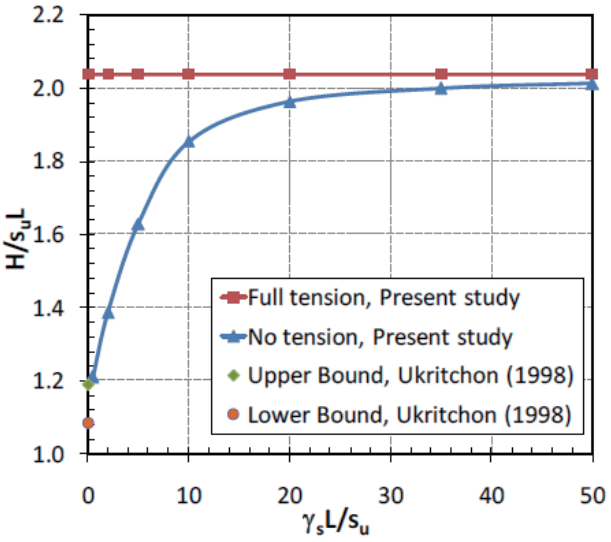


**Fig. 16 Dimensionless solutions of purely horizontal load**

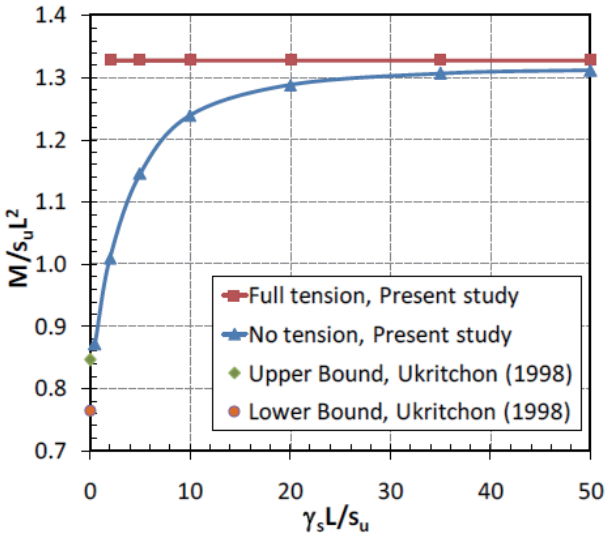


**Fig. 17 Dimensionless solutions of pure moment**

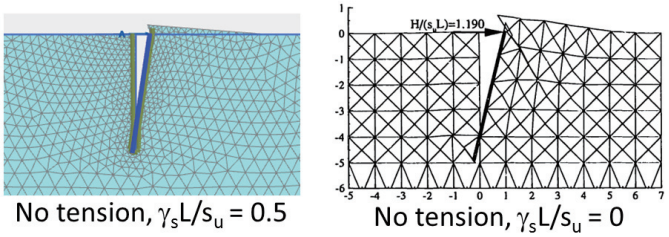


(a) Present study (b) Ukritchon (1998)

**Fig. 18 Deformed meshes between this study and Ukritchon (1998)**

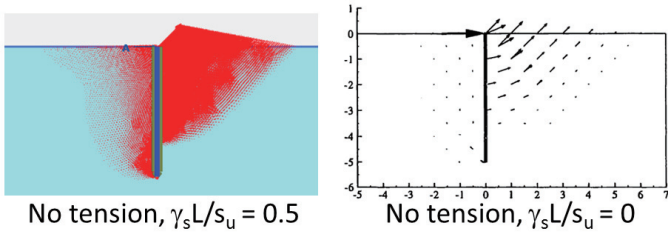


(a) Present study (b) Ukritchon (1998)

**Fig. 19 Incremental displacement between this study and Ukritchon (1998)**

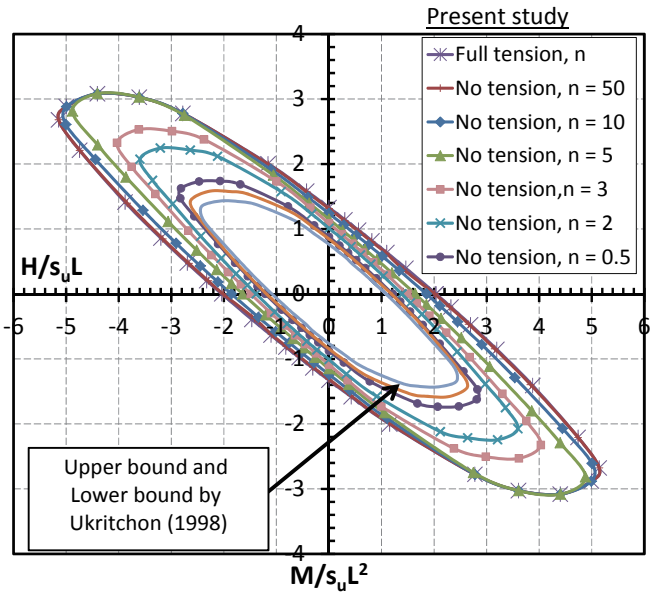


**Fig. 20 Failure envelopes of an embedded wall subjected to combined horizontal load and moment**

In addition, each failure envelope has the form of elliptical shape, which also rotates about $3\pi/4$ from the positive horizontal axis. However, the rotated ellipse is not symmetrical at its rotated major and minor axes. The non-symmetry of the ellipse happens at both ends of the major axis, resulting in a slightly distorted form of rotated ellipse. However, the distorted and rotated ellipse does hold the convexity condition, where the classical concept of failure envelope is still valid.

The size of the failure envelope of the full tension case is unaffected by the overburden factor, $\gamma_s L/s_u$. In contrast, that of the no tension case is controlled by $\gamma_s L/s_u$, where the higher ratio of $\gamma_s L/s_u$ is related to the larger size of the rotated ellipse. When $\gamma_s L/s_u$, > 50, the failure envelope of the no tension case practically converges to that of the full tension case. On the other hand, when $\gamma_s L/s_u$, < 0.5, the failure envelope of the no tension case shrinks to the smallest one that corresponds to the case of weight-less soil or zero soil unit weight. In general, the size of rotated failure envelope of the no tension case increases by about 40% when $\gamma_s L/s_u$ increases from 0 (weightless) to 2. Then, that size increases further by 40% as $\gamma_s L/s_u$ increases from 2 to 50. Thereafter, there is no change in the size of failure envelope when $\gamma_s L/s_u > 50$.

Figure 20 also shows the comparison of failure envelope by Ukritchon (1998) for the case of $\gamma_s L/s_u = 0$. It should be noted that the results of Ukritchon (1998) are based on the lower (LB) and upper bound (UB) finite element limit analyses, which do not consider the effect of soil unit weight ($\gamma_s = 0$). Very clearly, this figure revalidates the results of the present study with existing

solutions for the limiting case of weightless soil. The failure envelopes of the present study and those of Ukritchon (1998) have the similar form of a rotated nonsymmetrical ellipse, but their sizes are significantly different. The failure envelope of Ukritchon (1998) represents the smallest capacity since it corresponds to the envelope at the limiting condition of a weightless material or $\gamma_s L/s_u = 0$.

## 4. CONCLUSIONS

2D plane strain finite element analyses are employed to determine a new numerical solution of undrained lateral capacity of embedded underground walls subjected to combined horizontal load and moment in homogenous clay layer. Failure envelopes of $H/s_uL$ and $M/s_uL^2$ are developed as a function of $\gamma_s L/s_u$ for the cases of full tension and no tension. The analyses consider all aspects of lateral load including purely horizontal load, pure moment, and combined horizontal load and moment for all possible combinations. Unlike previous works in the past, a significant contribution of the present study is that a new numerical solution of failure envelope of laterally loaded walls under a horizontal load and moment are developed, which considers the effect of soil unit weight or the dimensionless overburden factor, $\gamma_s L/s_u$ in the practical ranges of 0.5 ~ 50. The results can be used for a stability evaluation of undrained lateral capacity of an underground wall with a sufficient horizontal length that is embedded in a deep homogeneous clay layer. Major findings of the proposed study are as follows:

1. Results of the present study are validated with existing solutions of the case, $\gamma_s L/s_u = 0$, where reasonable agreement can be established for all loadings including purely horizontal load, pure moment, and combined horizontal load and moment.
2. The failure of a laterally loaded wall with no tension occurs in such a way that there is a separation between soil and wall on the back side. The wall rotates about somewhere in between its mid-point and tip and does not undergo translational movement. An increase of $\gamma_s L/s_u$ ratio results in a lateral spreading of plastic zone on the back side of the wall. When $\gamma_s L/s_u$ has a large ratio or tends to reach to $\infty$, the failure mechanism of no tension case becomes that of full tension and is independent to an increase in $\gamma_s L/s_u$, where there is no separation between soil and wall.
3. For a general loading of $H$ and $M$, the failure envelope has the form of rotated ellipse with distortion at both ends. The size of failure envelope of the no tension case is controlled by the dimensionless overburden pressure, $\gamma_s L/s_u$. The increase of $\gamma_s L/s_u$ results in the increase of size of failure envelope until it converges to that of the full tension case. In other words, the case of weightless material or $\gamma_s L/s_u = 0$ gives rise to the smallest undrained lateral capacity of walls while that of the full tension case provides the largest undrained lateral capacity of walls for the no tension case when $\gamma_s L/s_u$ is extremely large or approaches infinity.

It is worth nothing that specific conditions of results should be limited to an underground wall with a sufficient horizontal length under a horizontal load and moment such that the plane strain assumption is valid in this study. In addition, the underground wall should not carry a vertical load in a large magnitude as compared to the horizontal load since there is no study of a general loading combination including vertical and horizontal loads and moment. If this is the case, a proper reduction of the failure envelope in H-M should be performed in order to take into account of the presence of a vertical load.

## REFERENCES


Blum, H. (1932). "Wirtschaftliche dalbenformen und deren berechnung." *Bautechnik*, **10**(5), 50–55.

Brinkgreve, R.B.J., Engin, E., and Swolfs, W.M. (2012). *Plaxis 2D 2012*, Netherlands.

Broms, B.B. (1964). "Lateral resistance of piles in cohesive soils." *Journal of the Soil Mechanics and Foundation*, **90**(2), 27–63.

Broms, B.B. (1965). "Design of laterally loaded piles." *Journal of the Soil Mechanics and Foundation*, **91**(3), 77–99.

Brown, D.A. and Shie, C.F. (1991). "Some numerical experiments with a three dimensional finite element model of a laterally loaded pile." *Computers and Geotechnics*, **12**, 149–162.

Butterfield, R. (1999). "Dimensional analysis for geotechnical engineering." *Géotechnique*, **49**(2), 357–366.

Chaudhry, A.R. (1994). *Static Pile-Soil-Pile Interaction in Offshore Pile Groups*, PhD Thesis, University of Oxford, UK.

Davisson, M.T. and Gill, H.L. (1963). "Laterally loaded piles in a layered soil." *Journal of the Soil Mechanics and Foundation*, **89**(3), 63–94.

Huang, M. and Huang, Q. (2007). "Ultimate lateral resistance of sheet pile walls by numerical lower bound analysis." *Chinese Journal of Geotechnical Engineering*, **29**(7), 988–994.

Ismael, N.F. (1990). "Behavior of laterally loaded bored piles in cemented sands." *Journal Geotechnical and Geoenvironmental Engineering*, **116**(11), 1678–1699.

Kimura, M., Adachi, T., Kamei, H., and Zhang, F. (1995). "3-D finite element analyses of the ultimate behavior of laterally loaded cast-in-place concrete piles." *Proceedings of the Fifth International Symposium on Numerical Models in Geomechanics*, NUMOG V, 589–594.

Klar, A. and Randolph, M.F. (2008). "Upper-bound and load-displacement solution for laterally loaded piles in clays based on energy minimization." *Géotechnique*, **58**(10), 815–820.

Matlock, H. and Reese, L.C. (1960). "Generalized solutions for laterally loaded piles." *Journal of the Soil Mechanics and Foundation*, **86**, 63–91.

Muqtadir, A. and Desai, C.S (1986). "Three dimensional analysis of a pile-group foundation." *International Journal for Numerical and Analytical Methods in Geomechanics*, **10**, 41–58.

Poulos, H.G. and Davis, E.H. (1980). *Pile Foundation Analysis and Design*, Wiley, New York.

Reese, L.C., Cox, W.R., and Koop, F.D. (1974). "Analysis of laterally loaded piles in sand." *Proceeding of 6th Offshore Technology Conference*, Houston, Texas, 473–483.

Reese, L.C. (1977). "Laterally loaded piles: Program documentation." *Journal Geotechnical and Geoenvironmental Engineering*, **103**(4), 287–305.

Reese, L.C., Wang, S.T., Isenhower, W.M., and Arrellaga, J.A. (2000). *Computer Program LPILE Plus Version 4.0 Technical Manual*, Ensoft, Inc., Austin, Texas.

Reese, L.C. and Van Impe, W.F. (2007). *Single Piles and Pile Groups Under Lateral Loading*, Taylor & Francis Group plc, London, UK.

Shen, W.Y. and Teh, C.I. (2002). "Analysis of laterally loaded pile groups using a variational approach." *Geotechnique*, **52**(3), 201–208.

Sloan, S.W. and Randolph, M.F. (1982). "Numerical prediction of collapse loads using finite element methods." *International Journal for Numerical and Analytical Methods in Geomechanics*, **6**, 47–76.

Ruigrok, J.A.T. (2010). *Laterally Loaded Piles Models and Measurements*, PhD Thesis, Delft University of Technology, Netherlands.

Trochanis, A.M., Bielak, J., and Christiano, P. (1991). "Simple model for analysis of one or two piles." *Journal Geotechnical and Geoenvironmental Engineering*, **117**(3), 448–466.

Ukritchon, B., Whittle, A.J. and Sloan, S.W. (1998). "Undrained limit analysis for combined loading of strip footings on clay." *Journal Geotechnical and Geoenvironmental Engineering*, **124**(1), 265–276.

Ukritchon, B. (1998). *Application of Numerical Limit Analyses for Undrained Stability Problems in Clay*, ScD Thesis, Massachusetts Institute of Technology, USA.

Wang, S. and Reese, L.C. (1993). *COM624P-Laterally Loaded Pile Analysis Program for the Microcomputer*, Version 2.0, FHWA-SA-91-048, U.S. DOT, Federal Highway Administration.

Yang, Z. and Jeremic, B. (2002). "Numerical analysis of pile behaviour under lateral loads in layered elastic–plastic soils." *International Journal for Numerical and Analytical Methods in Geomechanics*, **26**(14), 1385–1406.

Yang, Z. and Jeremic, B. (2005). "Study of soil layering effects on lateral loading behavior of piles." *International Journal for Numerical and Analytical Methods in Geomechanics*, **131**(6), 762–770.

Zhang, L. (2011). "Nonlinear analysis of laterally loaded rigid piles in cohesive soil." *International Journal for Numerical and Analytical Methods in Geomechanics*, **37**, 201–220.

Zhang, H.H. and Small, J.C. (2000). "Analysis of capped pile groups subjected to horizontal and vertical loads." *Computers and Geotechnics*, **26**, 1–21.